Unified constitutive modeling of rubber-like materials under diverse loading conditions

Gérard-Philippe Zéhil[a,*], Henri P. Gavin[a]

[a]*Department of Civil and Environmental Engineering, Duke University, 121 Hudson Hall, Box 90287, Research Drive, Durham, NC 27708-0287, United States*

Abstract

This paper presents a new constitutive model that unifies the behavioral characterizations of rubber-like materials in a broad range of loading regimes. The proposed model combines a selection of existing components that are known to reflect, with suitable accuracy, two fundamental aspects of rubber behavior in finite strain: (i) rate-independent softening under deformation, also known as the Mullins effect, and (ii) hyper-viscoelasticity, including at high strain rates. The evolution model is further generalized to account for multiple rates of internal dissipation (or material time-scales). Suitable means of identifying the system's parameters from simple uniaxial extension tests are explored. Several aspects of the model's behavior are shown in virtual experiments of uniaxial extension, at different stretch rates. A possible directional approach extending the model to handle softening induced anisotropy is briefly discussed.

Keywords: Finite strain, nonlinear viscoelasticity, stress-softening, constitutive modeling, rubber-like materials.

1. Introduction and background

Several classes of models have been proposed to characterize the constitutive behavior of rubber-like materials (e.g. Boyce and Arruda, 2000). Micro-mechanical models are founded on the physics of polymer chain networks and statistical methods (e.g. Arruda and Boyce, 1993; Drozdov and Dorfmann, 2004). Alternatively, phenomenological models rely on mathematical developments that are associated with conceptual representations or analogies with the purpose of replicating the material's behavior as observed at the macroscopic scale (e.g. Dorfmann and Ogden, 2004; Dorfmann and Pancheri, 2012; Gent, 1996; Hoo Fatt and Ouyang, 2007, 2008; Huber and Tsakmakis, 2000; Liu, 2010; Liu and Hoo Fatt, 2011; Ogden and Roxburgh, 1999; Pioletti et al., 1998). In some mixed approaches, constitutive equations are founded on macroscopic models that contain statistical parameters reflecting a certain representation of the microscopic structure (e.g. D'Ambrosio et al., 2008; De Tommasi et al., 2006; Horgan et al., 2004).

Most existing material descriptions were developed under specific loading conditions. For instance, in the work of Brown (1997), the nonlinear dynamic behavior of filled elastomers is characterized at small strain amplitudes. Alternatively, Hoo Fatt and Ouyang (2008) propose a finite strain constitutive model for virgin Styrene Butadiene rubber subjected to a high strain rate monotonic loading. Furthermore, Liu and Hoo Fatt (2011) present constitutive equations, in finite strain, for the dynamic response of rubber under cyclic loading while D'Ambrosio et al. (2008), De Tommasi et al. (2006) and many others (e.g Chagnon et al., 2004, 2006; Dorfmann and Ogden, 2004; Dorfmann and Pancheri, 2012; Horgan et al., 2004; Marckmann et al., 2002; Ogden and Roxburgh, 1999) focus on characterizing main features of the rate independent softening behavior of elastomers, i.e. the Mullins effect (Mullins, 1969). Valuable reviews of the Mullins effect as well as of existing viscoelastic and hyperelastic constitutive laws were provided by Diani et al. (2009), Boyce and Arruda (2000); Drapaca et al. (2007) and Marckmann and Verron (2006) respectively.

A careful inspection of the relevant literature furthermore reveals that a pertinent distinction can be made between: (i) models focusing on the rate independent softening behavior of the virgin material (e.g. D'Ambrosio et al., 2008;

*Corresponding author
Email address: gerard.zehil@duke.edu (Gérard-Philippe Zéhil)

De Tommasi et al., 2006), (ii) models describing its instantaneous response at high strain rates (e.g. Hoo Fatt and Ouyang, 2007, 2008), and (iii) models relating the repeatable dynamic behavior of the non-virgin material under cyclic loading (e.g. Liu and Hoo Fatt, 2011).

However, in many applications, rubbers are exposed to diverse loading conditions acting on the material in different states. This is the case, for instance, of elastomeric structural bearings and expansion joints which are subjected to prescribed displacements and tractions of various origins. While applied loads of increasing amplitude damage the polymer chain network and cause material softening, intermittent unloading conditions associated with temperature fluctuations can induce partial healing of the network and material stiffening by reentanglement and recross-linking of the chains. At an appropriate time scale, part of the applied load is monotonic and, depending on the previous loading history, may be acting on a partially-healed polymeric network. Conversely, cyclic loads typically engage a repeatable behavior of the non-virgin material. Both monotonic and cyclic loads can be slowly varying thus generating an equilibrium behavior (e.g. prescribed displacements due to material shrinking, creep, or thermal strains), or change rapidly hence engaging an instantaneous and rate-dependent response (e.g. passing train, emergency breaking, accidental shock, wind gust, or earthquake).

When rubber-like materials are subjected to mechanical loading cycles, their hyper-viscoelastic response experiences stiffness and damping degradations. Alternatively, full or partial recovery of the material's initial properties can occur following favorable changes in temperature and pressure. In many applications, the accurate prediction of such variations in the material's behavior is of paramount importance in addressing system reliability as well as human safety issues. Failing to account for such changes in behavior, with sufficient accuracy, can result in tragic outcomes with potentially disastrous consequences. Unfortunately, existing constitutive models have a restrictive range of application and limited predictive ability. Because in engineering practice material characterizations are often used unconnectedly while most viscoelastic models do not track the variations in the material's behavior, current designs involving rate dependent responses tend to overlook the Mullins effect and therefore rely on inaccurate predictions of the levels of degradation. This trend is further enhanced by the fact that, despite the abundance of tentative theories, consensus has not yet been reached on the actual physical sources of the Mullins effect (e.g. Diani et al., 2009). Consequently, the softening of rubbers under first deformation is frequently eluded in practical applications and no distinction is made between the primary response of the virgin material and its repeatable behavior under subsequent loadings.

In the current state of engineering practice, the prediction of a system's response under combined loading regimes, engaging a rate-dependent response and a softening behavior simultaneously, requires combining separate material models, each addressing a different aspect of material behavior. However, constitutive model libraries in commercial codes are far from exhaustive. Model combination rules and modalities are also limited, sometimes poorly documented and therefore opaque to the user. These facts often result in poorly-controlled modeling approximations which undermine prediction reliability and accuracy.

There are currently very few predictive models for the behavior of elastomers that also account for their degradation and can therefore be considered as potential candidates to be used for the safe design of engineered components. Three-dimensional finite strain behavioral laws comprising hyperelastic, viscoelastic and elastoplastic components were proposed by Lin and Schomburg (2003), Lion (1996) and Miehe and Keck (2000). These formulations are based on the theory of thermodynamics with internal state variables (Coleman and Gurtin, 1967) and retain different choices of such variables to characterize the evolution of internal dissipative processes. The Mullins stress-softening effect is assumed to act isotropically on all their components and it is accounted for within the framework of continuum damage mechanics (Kachanov, 1986; Lemaître, 1996) using a unique damage parameter. Despite their relative rheological completeness, these elaborate models continue to show notable imperfections in replicating true rubber behavior: common shortcomings in modeling the Mullins effect are described for instance by Diani et al. (2009) while further predictive limitations can be directly seen upon comparing observed and fitted behaviors (e.g. Lin and Schomburg (2003, figure 8);Lion (1996, figures 2.1 and 4.1)). Clearly, more alternatives are needed as much remains to be done in modeling elastomers.

2. Objective

In the absence of a unique and perfectly-accurate behavioral characterization of rubber-like materials, it is clear that significant improvements in design efficiency as well as substantial reductions in engineering resources and com-

putational costs may be achieved by the provision of a greater number of unified formulations, valid under multiple loading conditions. Developing such models further would also contribute to reaching higher levels of accuracy by eliminating the need for approximate prediction combination techniques.

In order to address these goals, alternative constitutive formulations must be considered and their modeling capabilities explored. Building on the current state of knowledge in modeling elastomers, this paper puts forward a new, mixed, three-dimensional, constitutive description of rubbers, in finite strain. The proposed model is based on a careful selection of preexisting components accurately reflecting key rubber behavior in two different loading regimes: (i) the rate-independent softening under deformation, also known as the Mullins effect, and (ii) hyper-viscoelasticity, including high strain rates. This new model complements the set of existing mixed formulations and is believed to have a significant potential in meeting the aforementioned needs, particularly in applications involving those two regimes.

3. Proposed model

Building on the work presented in D'Ambrosio et al. (2008) and De Tommasi et al. (2006) for a low strain rate characterization of the Mullins effect, as well as on existing high-speed constitutive modeling approaches, as addressed for instance in Hoo Fatt and Ouyang (2008), the new prototypical model shown in figure 1 is proposed as a unified description of the behavior of isotropic incompressible rubber-like materials, under multiple loading conditions.

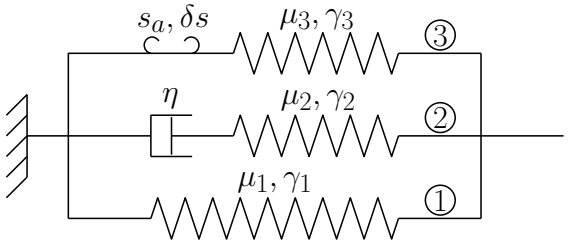

Figure 1: 1D representation of the full 3D prototypical model

The proposed model corresponds to an isotropic three-dimensional formulation in finite strain. Three model components contribute additively, in terms of stored energy and stress, to the global response: ① a permanent nonlinear hyperelastic component characterized by a stored energy function U_1, ② a permanent hyper-viscoelastic component characterized by a viscosity η and a stored energy function U_2 (i.e. a nonlinear Maxwell element), and ③ a non-permanent component composed of nonlinear hyperelastic links characterized by a distribution of activation and breaking thresholds, as well as a stored energy function U_3. The model is further generalized in section 9 to include multiple components of type ② and a possible directional approach extending the model to handle softening induced anisotropy is briefly discussed in section 10.

4. General kinematics

Addressing the hyper-viscoelastic component ② first, the total deformation gradient $\mathbf{F}_1$ is divided into a viscous component $\mathbf{F}_v$ and an elastic component $\mathbf{F}_2$ by means of a multiplicative decomposition

$$\mathbf{F}_1 = \mathbf{F}_2\mathbf{F}_v. \tag{1}$$

The intermediate configuration shown in figure 2 is generally not kinematically consistent. It corresponds to locally relaxed elements of continuum which are conceptually isolated from each other. Furthermore, the intermediate configuration is not unique: any combination of rigid body motions, in the local sense, would still yield an admissible alternative. Consequently, strain measures that are independent of the choice of intermediate configuration are used to describe the constitutive behavior of the material at hand.

Another set of multiplicative decompositions applies to the non-permanent links of type ③. As described in figure 3, the global deformation gradient $\mathbf{F}_1$ of each activable link is written as

$$\mathbf{F}_1 = \mathbf{F}_3\mathbf{F}_a, \tag{2}$$

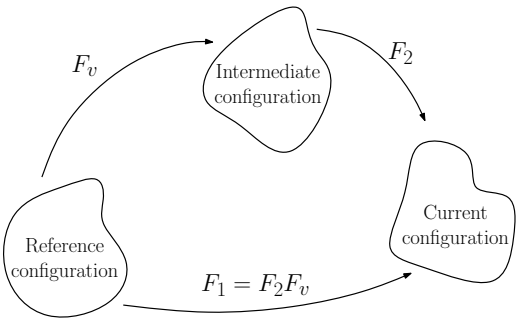

Figure 2: Multiplicative decomposition applying to links of type ②

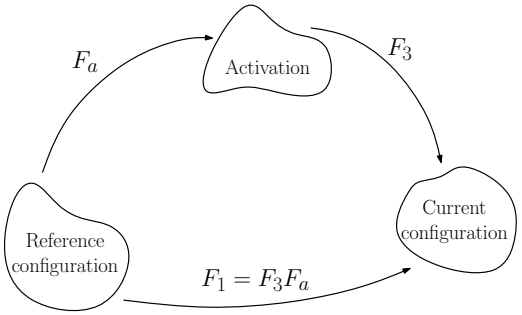

Figure 3: Multiplicative decomposition applying to links of type ③

where $\mathbf{F}_a$ is a partial deformation gradient that puts the link in a state of activation, while $\mathbf{F}_3$ corresponds to the complement of deformation associated with the strain energy U_3. The elastic energy stored in any given link of type ③ is lost when the link reaches a deformation gradient $\mathbf{F}_b$ putting it in a state of rupture.

5. Hyperelastic formulation

5.1. General theory

Assuming that each component undergoes an isochoric transformation, $J_j = \det(\mathbf{F}_j) = 1$ and the corresponding stored energy is a function of the first and second invariants of the appropriate measure of strain

$$U_j = U_j(I_{b_j}, II_{b_j}), \tag{3}$$

where $\mathbf{b}_j = \mathbf{F}_j\mathbf{F}_j^T$ is the left Cauchy-Green deformation tensor associated with the transformation defined by $\mathbf{F}_j$. The hyperelastic formulation used in this work builds on the fact that, for each component $j \in \{1, 2, 3\}$, the rate of change of the Lagrangian Green deformation tensor $\dot{\mathbf{E}}_j$ is work conjugate to the second Piola-Kirchhoff stress tensor $\mathbf{S}_j$ (i.e. the pull-back of the Cauchy stress tensor $\boldsymbol{\sigma}_j$)

$$\left.\begin{aligned} \dot{U}_j &= \left(\frac{\partial U_j}{\partial \mathbf{E_j}}\right)\!\mathbf{:}\dot{\mathbf{E}}_j \\ \dot{U}_j &= \mathbf{S}_j\mathbf{:}\dot{\mathbf{E}}_j \end{aligned}\right\} \Rightarrow \left(\frac{\partial U_j}{\partial \mathbf{E_j}} - \mathbf{S}_j\right)\!\mathbf{:}\dot{\mathbf{E}}_j = 0. \tag{4}$$

Due to incompressibility, the rate of change of J_j, which can be expressed in terms of the right Cauchy-Green deformation tensor $\mathbf{C}_j = \mathbf{F}_j^T\mathbf{F}_j$, is equal to zero (e.g. Bonet and Wood, 2008)

$$\dot{J}_j = \left(J_j\mathbf{C}_j^{-1}\right)\!\mathbf{:}\dot{\mathbf{E}}_j = 0. \tag{5}$$

Comparing equations (4) and (5) shows that both left hand sides are collinear, which, for $J_j = 1$, yields the following expression of the second Piola-Kirchhoff stress in component j

$$\mathbf{S}_j = \frac{\partial U_j}{\partial \mathbf{E}_j} + p_j\mathbf{C}_j^{-1}, \tag{6}$$

where the coefficient of proportionality p_j corresponds to an undetermined pressure term arising from incompressibility. Alternatively, a generic form of the Cauchy stress tensor in each component j is obtained by pushing forward $\mathbf{S}_j$, in expression (6), to the current configuration and applying the chain rule to $\partial U_j/\partial \mathbf{E}_j$ (see appendix A)

$$\boldsymbol{\sigma}_j = 2\left(\frac{\partial U_j}{\partial I_{b_j}} + I_{b_j}\frac{\partial U_j}{\partial II_{b_j}}\right)\mathbf{b}_j - 2\frac{\partial U_j}{\partial II_{b_j}}\mathbf{b}_j^2 - p_j\mathbf{I}. \tag{7}$$

It should be noted that the term $-p_j\mathbf{I}$ in expression (7) does not always correspond to the full stress axiator (i.e. the spherical part of $\boldsymbol{\sigma}_j$).

5.2. Specialized formulation

Numerous expressions of stored energy density functions are proposed in the literature (e.g. Marckmann and Verron, 2006). The dependence of U_i on I_{b_i} was found to be dominant in the case of incompressible rubber-like materials (e.g. Yeoh, 1990). The following form will be retained for the purposes of this work

$$U_j = \mu_j \left(I_{b_j} - 3\right)^{\gamma_j}, \tag{8}$$

where μ_j and γ_j are constant parameters, with $j \in \{1, 2, 3\}$. The underlying expression in (8) was reported capable of capturing the initially-stiff behavior of the material at high strain rates, without oscillating in the range of large deformations by Hoo Fatt and Ouyang (2008). Substituting (8) into (7) yields the corresponding Cauchy stress in each component

$$\boldsymbol{\sigma}_j = 2\mu_j\gamma_j \left(I_{b_j} - 3\right)^{\gamma_j - 1} \mathbf{b}_j - p_j \mathbf{I}. \tag{9}$$

6. Characterization of the non-permanent links

For simplicity, scalar activation and breaking criteria are retained for the non-permanent links: letting $s(\mathbf{F}_1)$ be a scalar function of the global deformation gradient $\mathbf{F}_1$, each link is activated when $s(\mathbf{F}_1)$ reaches its activation threshold s_a and breaks when $s(\mathbf{F}_1)$ exceeds its breaking threshold $s_b \geq s_a$. The active range of a non-permanent link is therefore characterized by the following expression

$$s_a = s(\mathbf{F}_1 = \mathbf{F}_a) \leq s(\mathbf{F}_1) \leq s(\mathbf{F}_1 = \mathbf{F}_b) = s_b, \tag{10}$$

where $\mathbf{F}_a$ and $\mathbf{F}_b$ correspond to the values taken by $\mathbf{F}_1$ when $s(\mathbf{F}_1) = s_a$ and $s(\mathbf{F}_1) = s_b$, respectively. Referring back to equation (2), the elastic deformation incurred by an active link is characterized by the partial deformation gradient $\mathbf{F}_3 = \mathbf{F}_1\mathbf{F}_a^{-1}$.

It is further assumed (see De Tommasi et al., 2006) that all the breakable links are active in a range of deformation of constant amplitude δs. Consequently, $s_b = s_a - \delta_s$ and only a marginal distribution needs to be defined for s_a. Figure 4 shows the proportions of active and broken links deduced from a generic probability density function $p(s_a)$ of the activation threshold: s_M is the maximum value taken by $s(\mathbf{F}_1)$ in the material's loading history, while s_f is the value of $s(\mathbf{F}_1)$ corresponding to the observed failure.

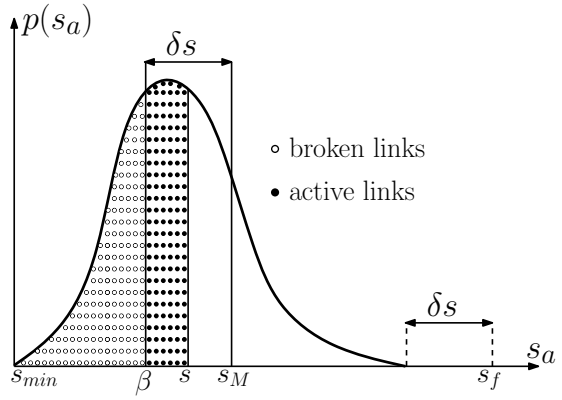

Figure 4: PDF of the activation threshold

Consistently with the form of hyperelastic potentials in expression (8) of section 5.2, a first-invariant-dependent measure of the state of the non-permanent links ③ is retained

$$I_a \leq s(\mathbf{F}_1) = I_{b_1} \leq I_a + \delta I. \tag{11}$$

The above choice is supported by a recent analysis conducted by Machado et al. (2010) on existing isotropic models for the Mullins effect, showing that the first invariant of strain is a good measure of stress-softening.

7. Global response

Components ①, ② and ③ of the proposed model (figure 1) contribute additively, in terms of internal energy and stress, to the global material response. The total stored energy density U and Cauchy stress $\boldsymbol{\sigma}$ are given by

$$U = U_1 + U_2 + \bar{U}_3, \tag{12}$$

$$\boldsymbol{\sigma} = \boldsymbol{\sigma}_1 + \boldsymbol{\sigma}_2 + \bar{\boldsymbol{\sigma}}_3. \tag{13}$$

where $\bar{U}_3$ and $\bar{\boldsymbol{\sigma}}_3$ correspond to the total contributions of the active links of type ③, obtained following De Tommasi et al. (2006) by integration over the active range $[\beta, s]$ (see figure 4), with $\beta = \min\{s, \max\{s_{min}, \max\{s, s_M\} - \delta s\}\}$, i.e.

$$\bar{U}_3 = \int_\beta^s U_3 p(s_a) ds_a, \tag{14}$$

$$\bar{\boldsymbol{\sigma}}_3 = \int_\beta^s \boldsymbol{\sigma}_3 p(s_a) ds_a. \tag{15}$$

8. Identification of model parameters

A feasible procedure is sought to determine the model parameters from simple uniaxial tension tests. In addition to the unknown probability density function $p(s_a)$ of the activation threshold for the links of type ③, relevant parameters are: η, δs, μ_j and γ_j for $j \in \{1, 2, 3\}$. In isochoric uniaxial tension, the generic deformation gradient $\mathbf{F}_j$ writes

$$\mathbf{F}_j = \begin{bmatrix} \lambda_j & 0 & 0 \\ 0 & \frac{1}{\sqrt{\lambda_j}} & 0 \\ 0 & 0 & \frac{1}{\sqrt{\lambda_j}} \end{bmatrix}, \tag{16}$$

where λ_j is the principal stretch in the direction of the applied traction σ_j. Substituting expression (16) into equation (9) and eliminating the pressure term p_j yields the generic scalar expression for σ_j

$$\sigma_j = 2\mu_j\gamma_j \left(\lambda_j^2 - \frac{1}{\lambda_j}\right)\left(I_{b_j} - 3\right)^{(\gamma_j - 1)}, \tag{17}$$

where I_{b_j} and λ_j are in one to one correspondence, since $I_{b_j} = \lambda_j^2 + 2/\lambda_j$ increases monotonically with the stretch $\lambda_j \geq 1$.

8.1. Low strain rate response

The material's quasi-static behavior is first examined in order to determine the parameters characterizing the distribution of activable links of type ③. When deformation occurs at a sufficiently low strain rate, the hyper-viscoelastic component ② flows while remaining fully relaxed. As shown in figure 5, the conceptual representation corresponding to this case reduces to branches ① and ③ of the prototypical model.

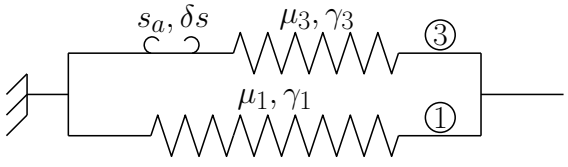

Figure 5: Reduced model at low strain rate

To simplify notations, let $\lambda = \lambda_1$ and $I(\lambda) = I_{b_1}(\lambda)$. A virgin dumbbell-shaped sample of rubber is loaded and unloaded, at a sufficiently low constant strain rate, up to increasing values of the maximum stretch λ_M corresponding to $I_M = I(\lambda_M)$. This may be done following the increasing triangular strain-history profile shown in figure 11(a) while

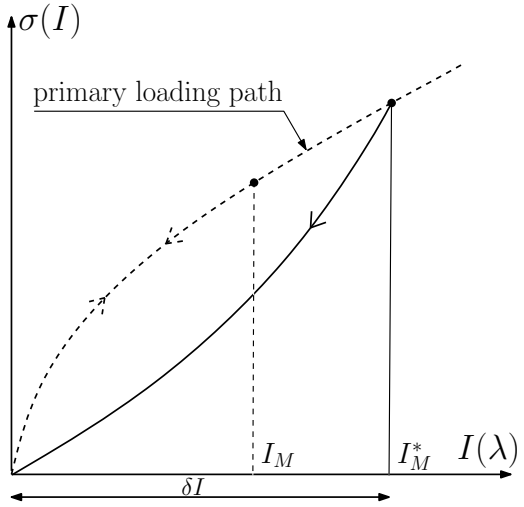

Figure 6: δI corresponds to the global elastic range of the virgin material

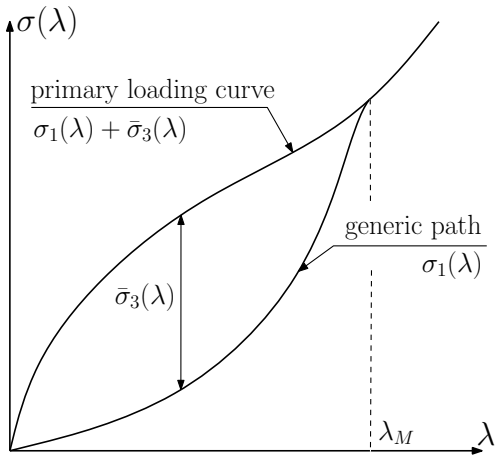

Figure 7: Illustration of material softening at low strain rate: $\sigma(\lambda) = \sigma_1(\lambda) + \bar{\sigma}_3(\lambda)$

keeping strain amplitudes globally small. As may be seen on figure 6, the parameter δI defines the global elastic range of the virgin material and may hence be determined from the value λ_M^* of the maximum stretch for which the unloading path differs from the primary loading curve: $\delta I = I_M^* = I(\lambda_M^*)$.

Referring back to figure 4, with $s = I$ and $\beta = \min\{I, \max\{I_{min}, \max\{I, I_M\} - \delta I\}\}$, equations (13) and (15) can be specialized to uniaxial extension, in the absence of component ② (i.e. $\sigma_2 = 0$), as follows

$$\sigma(\lambda) = \sigma_1(\lambda) + \bar{\sigma}_3(\lambda), \tag{18}$$

$$\bar{\sigma}_3(\lambda) = \int_\beta^I \sigma_3\left(\frac{\lambda(I)}{\lambda(I_a)}\right) p(I_a) dI_a. \tag{19}$$

Figure 7 illustrates equation (18) in relation to the Mullins effect (e.g. Diani et al., 2009; Mullins, 1969), i.e. the softening incurred by a virgin sample of rubber-like material upon deformation. The Cauchy stress σ_3 appears in equation (19) as a function of the ratio $\lambda(I)/\lambda(I_a)$ which corresponds to the one-dimensional formulation of the multiplicative decomposition applicable to links of type ③ and described in figure 3. By differentiating equations (18) and (19) with respect to λ, using Leibniz's rule, it can be shown that the probability density function of the activation threshold can be expressed as

$$p(I_a) = \frac{g\left(\lambda\left(I_a + \delta I\right)\right)}{\sigma_3\left(\frac{\lambda(I_a+\delta I)}{\lambda(I_a)}\right)}, \tag{20}$$

where $g(\lambda)$ can be interpolated from measured values of the slope $d\sigma/d\lambda$ at various λ_M along the primary loading curve (L) and the unloading path (U), as illustrated in figure 8

$$g(\lambda_M) = \frac{\lambda_M^2}{\left(2\lambda_M^3 - 1\right)}\left(\left.\frac{d\sigma}{d\lambda}\right|_{\lambda_M}^U - \left.\frac{d\sigma}{d\lambda}\right|_{\lambda_M}^L\right). \tag{21}$$

For this purpose, the increasing sawtooth strain-history profile shown in figure 11(b) may be applied at a very low strain rate, to a virgin sample of material, until rupture is reached.

Substituting equation (20) into (19) and then (19) into (18), the latter may be written as

$$\int_{I-\delta I}^I h\left(\lambda, I_a, \gamma_3\right) dI_a = \sigma(\lambda) - \sigma_1(\lambda), \tag{22}$$

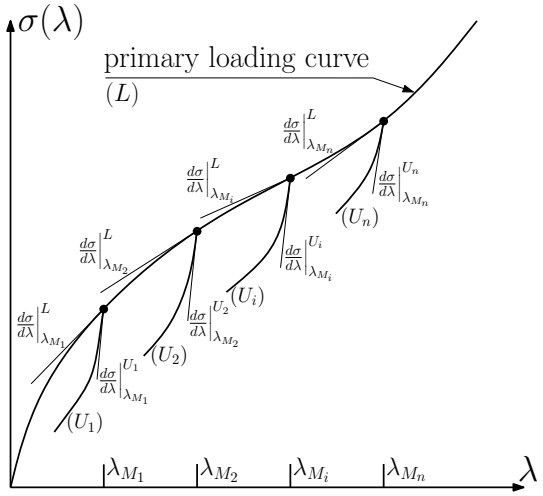

Figure 8: Determining data points $\left(\lambda_{M_i}, g\left(\lambda_{M_i}\right)\right)$

where the quantity on the right-hand-side can be deduced from the measured data (see figure 7). The parameter μ_3 simplifies in the expression of $h\left(\lambda, I_a, \gamma_3\right)$, which is given by the ratio

$$\frac{h\left(\lambda, I_a, \gamma_3\right)}{g\left(\lambda\left(I_a+\delta I\right)\right)}=\frac{\sigma_3\left(\frac{\lambda(I)}{\lambda(I_a)}\right)}{\sigma_3\left(\frac{\lambda(I_a+\delta I)}{\lambda(I_a)}\right)}. \tag{23}$$

The parameter γ_3 can be obtained from equation (22) by prediction error minimization. Once γ_3 is known, equation (20) can be normalized such that $\int_{I_{min}}^{I_f-\delta I} p(I_a)dI_a = 1$ which yields the parameter μ_3.

It may hence be concluded that all the parameters characterizing the distribution of activable links of type ③, including the probability density function of their activation threshold, can be determined by performing a multistage uniaxial tension test, at low strain rate, on a sample of virgin rubber. It remains to determine the parameters governing the behavior of the links of type ① and ②, which is precisely the goal of the following section.

8.2. Repeatable response

In this section, we consider the constitutive behavior of the non-virgin material in a range of deformation such that all remaining non-permanent links of type ③ are kept below their activation threshold. As shown in figure 9 the conceptual representation corresponding to this case reduces to branches ① and ② of the prototypical model.

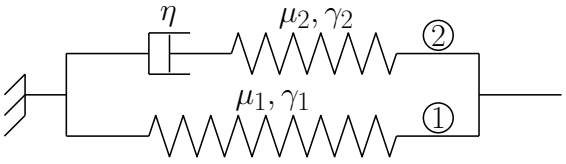

Figure 9: Reduced model in the repeatable range

8.2.1. Nonlinear hyper-viscoelastic formulation

With $j \in \{1, 2, v\}$, let $\mathbf{C}_j = \mathbf{F}_j^T\mathbf{F}_j$ and $\mathbf{b}_j = \mathbf{F}_j\mathbf{F}_j^T$ be right and left Cauchy-Green deformation tensors and denote by $\mathbf{E}_j$ and $\mathbf{e}_j$ the corresponding Green and Almansi strain tensors, respectively. Furthermore, let $\mathbf{T}$ and $\mathbf{\Gamma}$ be intermediate measures of the global stress and strain, i.e.

$$\mathbf{T} = \mathbf{F}_v\mathbf{S}\mathbf{F}_v^T = \mathbf{F}_2^{-1}\boldsymbol{\sigma}\mathbf{F}_2^{-T}, \tag{24}$$

$$\mathbf{\Gamma} = \mathbf{F}_v^{-T}\mathbf{E}_1\mathbf{F}_v^{-1} = \mathbf{F}_2^T\mathbf{e}_1\mathbf{F}_2. \tag{25}$$

The tensors $\mathbf{S}$ and $\boldsymbol{\sigma}$ in expression (24) correspond to measures of the global stress in the reference and current configurations respectively. Alternatively, $\boldsymbol{\Gamma}$ may be written as

$$\boldsymbol{\Gamma} = \frac{1}{2}\left(\mathbf{F}_2^T\mathbf{F}_2 - \mathbf{I}\right) + \frac{1}{2}\left(\mathbf{I} - \mathbf{F}_v^{-T}\mathbf{F}_v^{-1}\right) = \mathbf{E}_2 + \mathbf{e}_v, \tag{26}$$

where $\mathbf{E}_2$ and $\mathbf{e}_v$ are seen as intermediate measures of strain associated with the hyperelastic and viscous parts of component ②, respectively. Differentiating (26) with respect to time yields the relationship between the corresponding strain rates

$$\dot{\boldsymbol{\Gamma}} = \dot{\mathbf{E}}_2 + \dot{\mathbf{e}}_v. \tag{27}$$

The Lie derivative $\hat{\boldsymbol{\Gamma}}$ of $\boldsymbol{\Gamma}$ corresponds to the push-forward of $\dot{\mathbf{E}}_1$ to the intermediate frame, i.e.

$$\hat{\boldsymbol{\Gamma}} \triangleq \mathbf{F}_v^{-T}\dot{\mathbf{E}}_1\mathbf{F}_v^{-1} = \dot{\boldsymbol{\Gamma}} + \mathbf{l}_v^T\boldsymbol{\Gamma} + \boldsymbol{\Gamma}\mathbf{l}_v, \tag{28}$$

where $\mathbf{l}_v$ is the velocity gradient in the intermediate system of coordinates $\mathbf{x}_v$, i.e.

$$\mathbf{l}_v \triangleq \frac{\partial \mathbf{v}}{\partial \mathbf{x}_v} = \dot{\mathbf{F}}_v\mathbf{F}_v^{-1}. \tag{29}$$

Let $\mathcal{D}_{int}$ be the internal power dissipation due to the viscous effects. The second law of thermodynamics may be expressed pointwise, in the reference frame, by means of the Clausius-Planck inequality (e.g. Holzapfel, 2000)

$$\mathcal{D}_{int} = \mathbf{S}\!:\!\dot{\mathbf{E}}_1 - \dot{U} - \mathcal{S}\dot{\Theta} \geq 0, \tag{30}$$

where $\mathcal{S}$ is the entropy density, $\dot{\Theta}$ denotes the rate of change in temperature and $\dot{U}$ corresponds to the rate of change in free energy density. Assuming a constant temperature, inequality (30) specializes into

$$\mathcal{D}_{int} = \mathbf{S}\!:\!\dot{\mathbf{E}}_1 - \dot{U} \geq 0. \tag{31}$$

Expression (31) may be pushed forward to the intermediate frame as

$$\mathbf{T}\!:\!\hat{\boldsymbol{\Gamma}} - \dot{U} \geq 0. \tag{32}$$

The total Helmholtz free energy density U is then written as the sum of the energy densities stored in the hyperelastic portions of components ① and ②, each depending on the appropriate measure of strain

$$U = U_1(\mathbf{E}_1) + U_2(\mathbf{E}_2). \tag{33}$$

The rates of change of U_1 and U_2 may now be expressed as follows

$$\dot{U}_1 = \frac{\partial U_1}{\partial \mathbf{E}_1}\!:\!\dot{\mathbf{E}}_1, \tag{34}$$

$$\dot{U}_2 = \frac{\partial U_2}{\partial \mathbf{E}_2}\!:\!\dot{\mathbf{E}}_2. \tag{35}$$

Inverting equation (28) for $\dot{\mathbf{E}}_1$ and substituting into equation (34) yields the rate of change in $\dot{U}_1$ as

$$\dot{U}_1 = \left(\mathbf{F}_v\frac{\partial U_1}{\partial \mathbf{E}_1}\mathbf{F}_v^T\right)\!:\!\hat{\boldsymbol{\Gamma}}. \tag{36}$$

On the other hand, manipulating equations (27) and (28) it can be shown that $\dot{\mathbf{E}}_2$ satisfies

$$\dot{\mathbf{E}}_2 = \hat{\boldsymbol{\Gamma}} - \mathbf{d}_v - \mathbf{l}_v^T\mathbf{E}_2 - \mathbf{E}_2\mathbf{l}_v, \tag{37}$$

where $\mathbf{d}_v$ is the rate of deformation of the viscous component in ②

$$\mathbf{d}_v = \frac{1}{2}\left(\mathbf{l}_v + \mathbf{l}_v^T\right) = \dot{\mathbf{e}}_v + \mathbf{l}_v^T\mathbf{e}_v + \mathbf{e}_v\mathbf{l}_v. \tag{38}$$

Comparing the right-hand-sides of expressions (28) and (38) shows that $\mathbf{d}_v$ is the Lie derivative of $\mathbf{e}_v$. Plugging equation (38) into (37) and then (37) into (35) yields the rate of change in $\dot{U}_2$ as

$$\dot{U}_2 = \frac{\partial U_2}{\partial \mathbf{E}_2} : \hat{\mathbf{\Gamma}} - \left(\mathbf{C}_2 \frac{\partial U_2}{\partial \mathbf{E}_2} \right) : \mathbf{d}_v, \tag{39}$$

where, in the case of an isotropic material, the Mendel stress ($\mathbf{C}_2 \partial U_2 / \partial \mathbf{E}_2$) is symmetric. Defining intermediate measures of partial stress in components ① and ② respectively as

$$\mathbf{T}_1 = \mathbf{F}_v \frac{\partial U_1}{\partial \mathbf{E}_1} \mathbf{F}_v^T \quad \text{and} \quad \mathbf{T}_2 = \frac{\partial U_2}{\partial \mathbf{E}_2}, \tag{40}$$

then substituting equation (36) and (39) into (32) yields the following inequality (e.g. Hoo Fatt and Ouyang, 2008; Huber and Tsakmakis, 2000)

$$\mathcal{D}_{int} = [\mathbf{T} - (\mathbf{T}_1 + \mathbf{T}_2)] : \hat{\mathbf{\Gamma}} + [\mathbf{C}_2 \mathbf{T}_2] : \mathbf{d}_v \geq 0, \tag{41}$$

where the history of the global deformation gradient $\mathbf{F}_1$, and hence the tensorial quantity $\hat{\mathbf{\Gamma}}$, can be chosen arbitrarily. A standard procedure due to Coleman and Noll (1963); Coleman and Gurtin (1967) is applied to satisfy inequality (41):

- In the particular case where the rate of deformation of the viscous component is equal to zero (i.e. $\mathbf{d}_v = \mathbf{0}$), the transformation process is reversible and inequality (41) reduces to

$$\mathcal{D}_{int} = [\mathbf{T} - (\mathbf{T}_1 + \mathbf{T}_2)] : \hat{\mathbf{\Gamma}} = 0. \tag{42}$$

  Equality (42) is satisfied for every choice of $\mathbf{F}_1$ if and only if

$$\mathbf{T} = \mathbf{T}_1 + \mathbf{T}_2 \quad \Longleftrightarrow \quad \boldsymbol{\sigma} = \boldsymbol{\sigma}_1 + \boldsymbol{\sigma}_2. \tag{43}$$

- Assuming that local equilibrium (43) is satisfied in the general case where $\mathbf{d}_v \neq \mathbf{0}$, expression (41) reduces to

$$(\mathbf{C}_2 \mathbf{T}_2) : \mathbf{d}_v \geq 0. \tag{44}$$

It is noteworthy that inequality (44) is independent of the choice of intermediate configuration. For an isotropic material, the "Mandel" stress tensor $\mathbf{C}_2 \mathbf{T}_2$ is symmetric. The following evolution law was proposed by Huber and Tsakmakis (2000) as a simple condition that satisfies inequality (44)

$$\mathbf{d}_v = \frac{1}{\eta} (\mathbf{C}_2 \mathbf{T}_2)^d, \tag{45}$$

where the superscript $(.)^d$ denotes a deviatoric component. Using (45) and denoting the velocity gradients by $\mathbf{l}_j = \dot{\mathbf{F}}_j \mathbf{F}_j^{-1}$, it can be shown that

$$\dot{\mathbf{b}}_2 = \mathbf{l}_1 \mathbf{b}_2 + \mathbf{b}_2 \mathbf{l}_1^T - \frac{2}{\eta} \mathbf{b}_2 \boldsymbol{\sigma}_2^d. \tag{46}$$

8.2.2. Practical subsystem identification (saturation method)

Following a procedure proposed by Hoo Fatt and Ouyang (2008), the parameters μ_1 and γ_1 can be determined first by a nonlinear regression analysis based on equation (17) with $j = 1$. The corresponding equilibrium response σ_1 (see figure 10) is obtained by loading a non-virgin material sample in uniaxial extension at a suitably low constant strain rate (ramp-up) and holding it at increasing values of constant strain (plateau) to allow for relaxation of the overstress σ_2 in component ②. This combined constant strain rate and incremental stress relaxation test is illustrated in figure 11(c). Intervals of constant strain must be adjusted according to the material's relaxation spectrum.

The subsystem in figure 9 may be further identified using monotonic strain-history profiles of (preferably) constant strain rates (see figure 11(d)). Subjecting the sample to a sufficiently high strain rate will induce locking of the viscous component (i.e. $\lambda_v = 0$) and yield the saturation response σ_{sat} (see figure 10) corresponding to $\lambda_1 = \lambda_2 = \lambda$. A

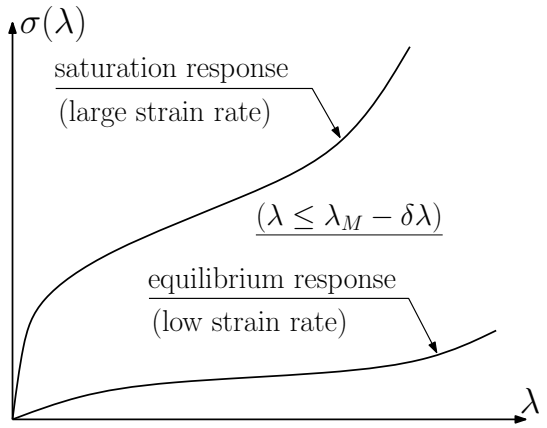

Figure 10: The material's repeatable response lives between the equilibrium curve and the saturation curve

nonlinear regression analysis based on equation (17) with $\sigma_{sat} = \sigma_1(\lambda) + \sigma_2(\lambda)$ determines the parameters μ_2 and γ_2. The remaining parameter η can be determined at any intermediate elongation rate $\dot{\lambda}_1$ from equation (46) which, in uniaxial tension writes

$$\eta = \frac{2\lambda_1\lambda_2\sigma_2}{3\left(\dot{\lambda}_1\lambda_2 - \lambda_1\dot{\lambda}_2\right)}. \tag{47}$$

The viscosity η may show to be practically constant. Conversely, as reported for instance by Hoo Fatt and Ouyang (2008) for Styrene Butadiene, viscosity may be governed by deformation. In the latter case, the dependences on deformation amplitude and rate can be characterized using the state variables I_{b_1} and I_{b_2} respectively: proposed analytical expressions of $\eta\left(I_{b_1}, I_{b_2}\right)$ may be fitted to the observed results using nonlinear regression analysis.

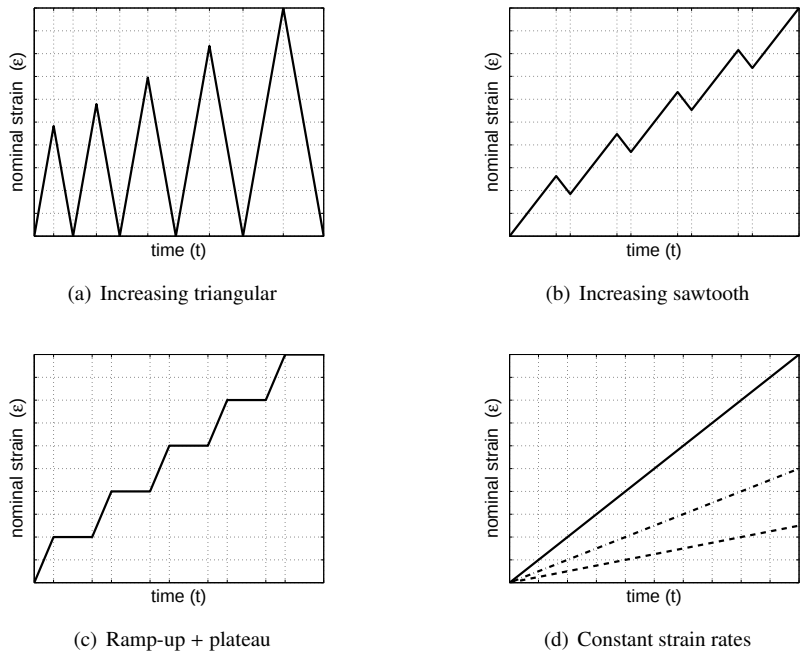

(a) Increasing triangular

(b) Increasing sawtooth

(c) Ramp-up + plateau

(d) Constant strain rates

Figure 11: Examples of strain-history profiles suitable for material characterization in uniaxial extension

8.2.3. Practical subsystem identification (PEM method)

The methodology described in section 8.2.2 relies on an ability to achieve sufficiently high (constant) strain rates, in order to provoke saturation of the viscous component. Practically obtainable rates using commercially available servohydraulic test machines are limited. Higher rates in traction can be acheived with specifically-designed testing apparatus like the modified Charpy impact machine described by Hoo Fatt and Ouyang (2008) or the falling weight apparatus proposed by Roland (2006).

In case technical difficulties are encountered in this regard, one alternative approach would be to determine the parameters of components ① and ② simultaneously, by prediction error minimization (PEM) with respect to the repeatable behavior, as observed within the range of achievable strain rates. Indeed, expressions for the overstress σ_2 resulting from equations (17) and (47) may be equated to obtain a nonlinear ordinary differential equation (ODE) in the elastic component of the stretch $\lambda_2(t)$ in branch ②. For the purpose of numerical computations, a convenient ODE formulation is obtained in terms of the proxy variable $y = \lambda_1/\lambda_2$, i.e.

$$\frac{dy}{dt} = \frac{2y}{3\eta}\sigma_2\left(\frac{\lambda_1}{y}\right). \tag{48}$$

Given a global stretch history $\lambda_1(t) = \lambda(t)$, the aforementioned ODE can be solved for $\lambda_2(t)$ using current iterates for the model's parameters. The predicted history of the total stress $\sigma(t)$ is obtained by adding its two components evaluated using expressions ((17) with $j \in \{1, 2\}$) and compared, at each iteration, to the observed response.

9. Generalized model

The prototypical model shown in figure 1 can be generalized further to include a number $n \geq 1$ of nonlinear hyper-viscoelastic Maxwell elements of type ②. The procedure described in section 8.1 for characterizing the low strain rate response remains unchanged. However, for $n > 1$, the saturation method of section 8.2.2 cannot be applied to identify the repeatable behavior. A generalized version of the alternative method based on prediction error minimization (see section 8.2.3) may be used instead.

The i^{th} type ② Maxwell element ($1 \leq i \leq n$) is characterized by a viscosity η_i and a free energy density $U_{2,i}$. It is further associated with a proper intermediate configuration $\mathcal{I}_i$ and the corresponding multiplicative decomposition

$$\mathbf{F}_1 = \mathbf{F}_{2,i}\mathbf{F}_{v,i}. \tag{49}$$

Following a similar derivation to the one presented in section 8.2.1, it can be shown that inequality (41) generalizes into a set of n equivalent inequalities of the form

$$\left[\mathbf{T}^i - \left(\mathbf{T}^i_1 + \sum_{j=1}^{n}\mathbf{T}^i_{2,j}\right)\right]\!:\hat{\mathbf{\Gamma}}^i + \sum_{j=1}^{n}\left(\mathbf{C}_{2,j}\mathbf{T}^j_{2,j}\right)\!:\mathbf{d}_{v,j} \geq 0, \tag{50}$$

where the partial stress $\mathbf{T}^i_{2,j}$ in the j^{th} hyperelastic component and the total stress $\mathbf{T}^i$ are expressed in $\mathcal{I}_i$. The quantity $\hat{\mathbf{\Gamma}}^i$ corresponds to the Lie derivative of the i^{th} intermediate measure of global strain and $\mathbf{d}_{v,j}$ denotes the rate of deformation of the j^{th} viscous component, expressed in $\mathcal{I}_j$. Following the Coleman-Noll procedure, expression (50) reveals the general additivity of partial stresses, i.e.

$$\mathbf{T}^i = \mathbf{T}^i_1 + \sum_{j=1}^{n}\mathbf{T}^i_{2,j} \;\; (\forall j) \quad \Longleftrightarrow \quad \boldsymbol{\sigma} = \boldsymbol{\sigma}_1 + \sum_{j=1}^{n}\boldsymbol{\sigma}_{2,j}, \tag{51}$$

as well as a generalized dissipation inequality:

$$\mathcal{D}_{int} = \sum_{j=1}^{n}\left(\mathbf{C}_{2,j}\mathbf{T}^j_{2,j}\right)\!:\mathbf{d}_{v,j} \geq 0. \tag{52}$$

Inequality (52) can be satisfied simply, by retaining for the n viscous components, uncoupled evolution laws of the form given by expression (45), i.e.

$$\mathbf{d}_{v,j} = \frac{1}{\eta_j}\left(\mathbf{C}_{2,j}\mathbf{T}^j_{2,j}\right)^d. \tag{53}$$

Using the laws in (53), expressions (46), (47) and (48) can be generalized to the j^{th} component of type ② as follows

$$\dot{\mathbf{b}}_{2,j} = \mathbf{l}_1\mathbf{b}_{2,j} + \mathbf{b}_{2,j}\mathbf{l}_1^T - \frac{2}{\eta_j}\mathbf{b}_{2,j}\boldsymbol{\sigma}^d_{2,j}, \tag{54}$$

$$\eta_j = \frac{2\lambda_1\lambda_{2,j}\sigma_{2,j}}{3\left(\dot{\lambda}_1\lambda_{2,j} - \lambda_1\dot{\lambda}_{2,j}\right)}, \tag{55}$$

$$\frac{dy_j}{dt} = \frac{2y_j}{3\eta_j}\sigma_{2,j}\left(\frac{\lambda_1}{y_j}\right). \tag{56}$$

In a stretch-driven uniaxial extension test, the global stretch history $\lambda_1(t) = \lambda(t)$ is known. Assuming an initial guess for the parameters characterizing component ① and the components of type ②, the n uncoupled ODE's given by expression (56) can be solved for the elastic portions $\lambda_{2,i}(t)$ of the stretch in each Maxwell element. The partial stress in each hyperelastic component can be determined from its constitutive equation, i.e. equation (17) in the present case. A predicted history of the total stress $\boldsymbol{\sigma}(t)$ is obtained by summation according to expression (51). The difference between the predicted response and the observed response can be minimized by iterating on the model's parameters.

10. Mullins effect induced anisotropy

10.1. A brief overview

Based on considerations of material symmetry, but also on the implicit assumption of a directional network alteration (as opposed to an isotropic one), Horgan et al. (2004) argue that the damage associated with the Mullins effect is inherently anisotropic and briefly discuss a tensorial approach to account for this anisotropy. Experimental data (e.g. Dargazany and Itskov, 2009; Diani et al., 2006; Dorfmann and Pancheri, 2012; Itskov et al., 2006; Machado et al., 2012) confirm that stress softening introduces some anisotropy in the material response. Diani et al. (2006) and Dargazany and Itskov (2009) present micromechanical directional models to handle softening induced anisotropy. The potential of several finite-directional models in reflecting the behavioral anisotropy induced by the Mullins effect in initially isotropic hyperelastic materials is tested by Gillibert et al. (2010), based on the models' initial anisotropy and their ability to replicate the behavior of a full (i.e. infinite-directional) network. Dorfmann and Pancheri (2012) build on the tensorial approach outlined by Horgan et al. (2004) and derive a simple phenomenological model accounting for stress softening and changes in material symmetry. The model applies, in its current form, to pure homogeneous deformations; however, it may be extended to more general loading conditions by the addition of an evolution law.

10.2. Outline of model extension

The formulation characterizing component ③ of the mixed model presented in this paper can also be extended, in several ways, to handle softening induced anisotropy. A possible directional approach, preserving the form of stored energy density given by equation (8), with $j = 3$, as well as the scalar measure of the active range specified in expression (11), is outlined hereafter.

To this end, component ③ can be considered as a collection of incompressible directional networks. Each network $\mathcal{N}^{(u)}$ has an elongated shape; it is oriented in a given direction of unit vector $\mathbf{u}$ and comprises a very large number of activable/breakable links characterized by a distribution of activation thresholds similar to the one illustrated on figure 4. It is further assumed that, under the global deformation gradient $\mathbf{F} = \mathbf{F}_1$, each directional network $\mathcal{N}^{(u)}$ of component ③ softens isotropically while subjected to a uniaxial deformation characterized by the stretch $\lambda^{(u)}$ resulting from $\mathbf{F}$ in direction $\mathbf{u}$, i.e.

$$\lambda^{(u)} = \sqrt{(\mathbf{Fu})\,.\,(\mathbf{Fu})} = \sqrt{\mathbf{u}^T\mathbf{C}\mathbf{u}}, \tag{57}$$

where $\mathbf{C} = \mathbf{F}^T\mathbf{F}$. Under these conditions, the scalar measure of deformation of network $\mathcal{N}^{(u)}$ is given by the quantity $I^{(u)} = \lambda^{(u)2} + 2/\lambda^{(u)}$. As is usually the case in directional models, the number of spatial directions $\mathcal{N}^{(u)}$ can be finite or infinite. An infinite-directional formulation is outlined below in analytical form, which can be numerically integrated on the surface of a unit sphere, for instance, using sets of collocation directions and weights determined by Bažant and Oh (1986).

The stored energy density and the principal Cauchy stress in the direction of the current unit vector $\mathbf{Fu}/\lambda^{(u)}$, associated with an active link of network $\mathcal{N}^{(u)}$, are given by

$$U_3^{(u)} = \mu_3 \left(I_3^{(u)} - 3\right)^{\gamma_3} = \mu_3 \left(\lambda_3^{(u)2} + \frac{2}{\lambda_3^{(u)}} - 3\right)^{\gamma_3}, \tag{58}$$

$$\sigma_3^{(u)} = \lambda_3^{(u)} \frac{dU_3^{(u)}}{d\lambda_3^{(u)}} + p_3^{(u)} = 2\left(\lambda_3^{(u)2} - \frac{1}{\lambda_3^{(u)}}\right) \frac{dU_3^{(u)}}{dI_3^{(u)}} + p_3^{(u)}, \tag{59}$$

where $p_3^{(u)}$ is an undetermined pressure term arising from incompressibility. All active links in a given directional network $\mathcal{N}^{(u)}$ contribute additively, in terms of stored energy density and stress, to the elastic response of the network. The latter is hence found by summation over the active range, i.e.

$$\bar{U}_3^{(u)} = \int_{\beta^{(u)}}^{I_3^{(u)}} U_3^{(u)} p(I_a) dI_a, \tag{60}$$

$$\boldsymbol{\sigma}_3^{(u)} = \frac{1}{\lambda^{(u)2}} \int_{\beta^{(u)}}^{I_3^{(u)}} \sigma_3^{(u)} p(I_a) dI_a \, (\mathbf{Fu}) \otimes (\mathbf{Fu}). \tag{61}$$

Expressions for the total elastic response of component ③ are finally obtained by integrating equations (60) and (61) on the surface of a unit sphere $\mathcal{S}$

$$U_3 = \frac{1}{4\pi} \int_{\mathcal{S}} \left(\int_{\beta^{(u)}}^{I_3^{(u)}} U_3^{(u)} p(I_a) dI_a \right) d\mathcal{S}^{(u)}, \tag{62}$$

$$\boldsymbol{\sigma}_3 = 2\mathbf{F} \left[\frac{1}{4\pi} \int_{\mathcal{S}} \left(\int_{\beta^{(u)}}^{I_3^{(u)}} \left(1 - \frac{1}{\lambda_3^{(u)3}}\right) \frac{dU_3^{(u)}}{dI_3^{(u)}} \frac{p(I_a)}{\lambda\,(I_a)^2} dI_a \, \mathbf{u} \otimes \mathbf{u} \right) d\mathcal{S}^{(u)} \right] \mathbf{F}^T + p_3 \mathbf{I}. \tag{63}$$

Assuming a suitable analytical expression for $p(I_a)$ in terms of parameters, the anisotropic stress response of component ③ to a given global deformation history $\mathbf{F}(t)$ can be predicted using equation (63). Consequently, the model's parameters can be fitted to experimental data by minimizing the prediction error.

11. Example

Referring to figure 1, with a single component of type ②, the following set of numerical parameters is chosen to illustrate some aspects of the isotropic model's behavior in uniaxial extension at different strain rates: $\mu_1 = 1.1$ MPa, $\gamma_1 = 0.8$, $\mu_2 = 3.3$ MPa, $\gamma_2 = 1.1$, $\mu_3 = 19.8$ MPa, $\gamma_3 = 0.7$, $\eta = 0.05$ MPa.s and $\delta I = 5$. The activation threshold I_a of the first invariant of global strain is taken to follow the probability density function of a beta distribution, which is bounded (see e.g. Ang and Tang, 2007), i.e.

$$p(I_a) = \frac{1}{\beta(p,q)} \frac{(I_a - I_{a,min})^{p-1} (I_{a,max} - I_a)^{q-1}}{(I_{a,max} - I_{a,min})^{p+q-1}}, \tag{64}$$

where $I_a \in [I_{a,min}, I_{a,max}]$ with $I_{a,min} = 3$ and $I_{a,max} = \left(I_f - \delta I\right) = 100$. The standard *beta function* appearing in the denominator of expression (64) is given by

$$\beta(p,q) = \int_0^1 x^{p-1}(1-x)^{q-1} dx. \tag{65}$$

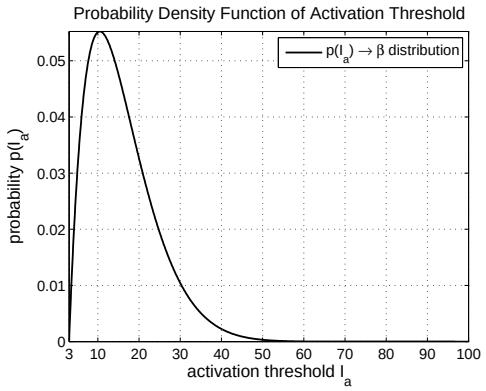

Figure 12: Assumed probability density function of the activation threshold I_a characterizing the links of type ③: $p\,(I_a)$ follows a β-distribution with $p = 3$, $q = 13$ and $I_a \in [1, 100]$.

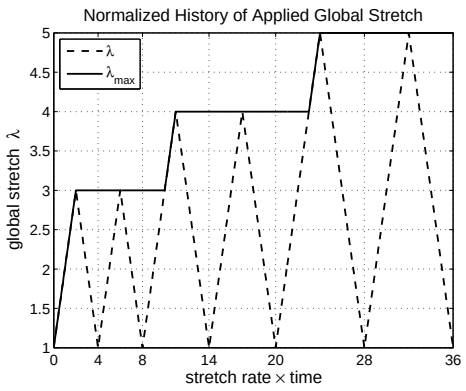

Figure 13: Virgin models are subjected, in uniaxial extension, to a standardized history of global stretch at different stretch rates: $\dot{\lambda}_1 = 0.1\ \mathrm{s}^{-1}$, $200\ \mathrm{s}^{-1}$ and $600\ \mathrm{s}^{-1}$.

Figure 12 shows the probability density function of I_a for $p = 2$ and $q = 13$, which is positively skewed.

The three-component model is subjected, uniaxially, to the normalized history of global stretch defined in figure 13: three sets of two stretch-driven loading cycles are applied to the virgin model, at increasing stretch amplitudes $\lambda_M = 3$, 4 and 5. This virtual experiment is repeated at three different stretch rates $\dot{\lambda}_1 = 0.1\ \mathrm{s}^{-1}$, $200\ \mathrm{s}^{-1}$ and $600\ \mathrm{s}^{-1}$.

The model's response to the lowest stretch rate $\dot{\lambda}_1 = 0.1\ \mathrm{s}^{-1}$ can be seen on the set of figures 14(a). At this rate, the virtual experiment is performed sufficiently slowly, with respect to the material's internal time-scale, for the viscous subcomponent to flow at nearly the same rate and undertake most of the applied stretch. Consequently, the elastic subcomponent of element ② remains unloaded with $\lambda_2 \approx 0$ and $\sigma_2 \approx 0$. On the other hand, the history of the stress in component ③ is consistent with the deterioration process to which the corresponding links are subjected to. It can be noted for instance that, over each set (i) of two successive loading cycles of same stretch amplitude λ_{M_i}, $\sigma_3(t)$ has a weaker intensity preceding the instant at which the maximum applied stretch λ_{M_i} occurs, and that it follows the same pattern past that point. When subjected to a sufficiently low rate of stretch, the system behaves as the reduced model shown in figure 5 and hence undergoes a pure Mullins effect.

The sets of figures 14(b) and 14(c) show the model's behavior at higher stretch rates: $\dot{\lambda}_1 = 200\ \mathrm{s}^{-1}$ and $600\ \mathrm{s}^{-1}$ respectively. The responses of components ① and ③ in a stretch-driven experiment are clearly rate-independent. Element ② however, behaves differently: the internal rate of dissipation of its viscous subcomponent being limited, the elastic subcomponent, which responds instantaneously, undertakes larger parts λ_2 of the applied stretch λ_1, at larger stretch rates. Upon unloading, and despite a state of global extension with $\lambda_1 \geq 1$, the delayed viscous response results in the compression of component ② with $\lambda_2 \leq 1$ and $\sigma_2 \leq 0$.

Further, it is interesting to note that, at sufficiently high strain rates, the peak in total stress $\sigma(t)$ drops significantly between the first and the second loading cycles. In the present case, this is less apparent in subsequent sets of larger global stretch amplitude. However, the magnitude of such drops can be modulated by changing the stretch rate or introducing time delays between successive loading sets. This phenomenon is clearly a manifestation of the model's viscoelastic behavior and should not be mistaken with stress-softening or damage.

12. Conclusions

A new three-dimensional multi-regime evolution model for rubber-like materials is presented in this work. The proposed model is based on a selection of existing components and unifies two major aspects of rubber behavior, in large deformations: nonlinear viscoelasticity and the Mullins effect. The prototypical formulation is further generalized to include multiple nonlinear Maxwell elements accounting for several internal material time-scales. A detailed analysis provides practical means of determining the model's parameters from simple uniaxial extension tests. A numerical example illustrates several aspects of the model's behavior in uniaxial extension, at different stretch rates. A possible directional approach extending the model to handle Mullins effect induced anisotropy is briefly discussed.

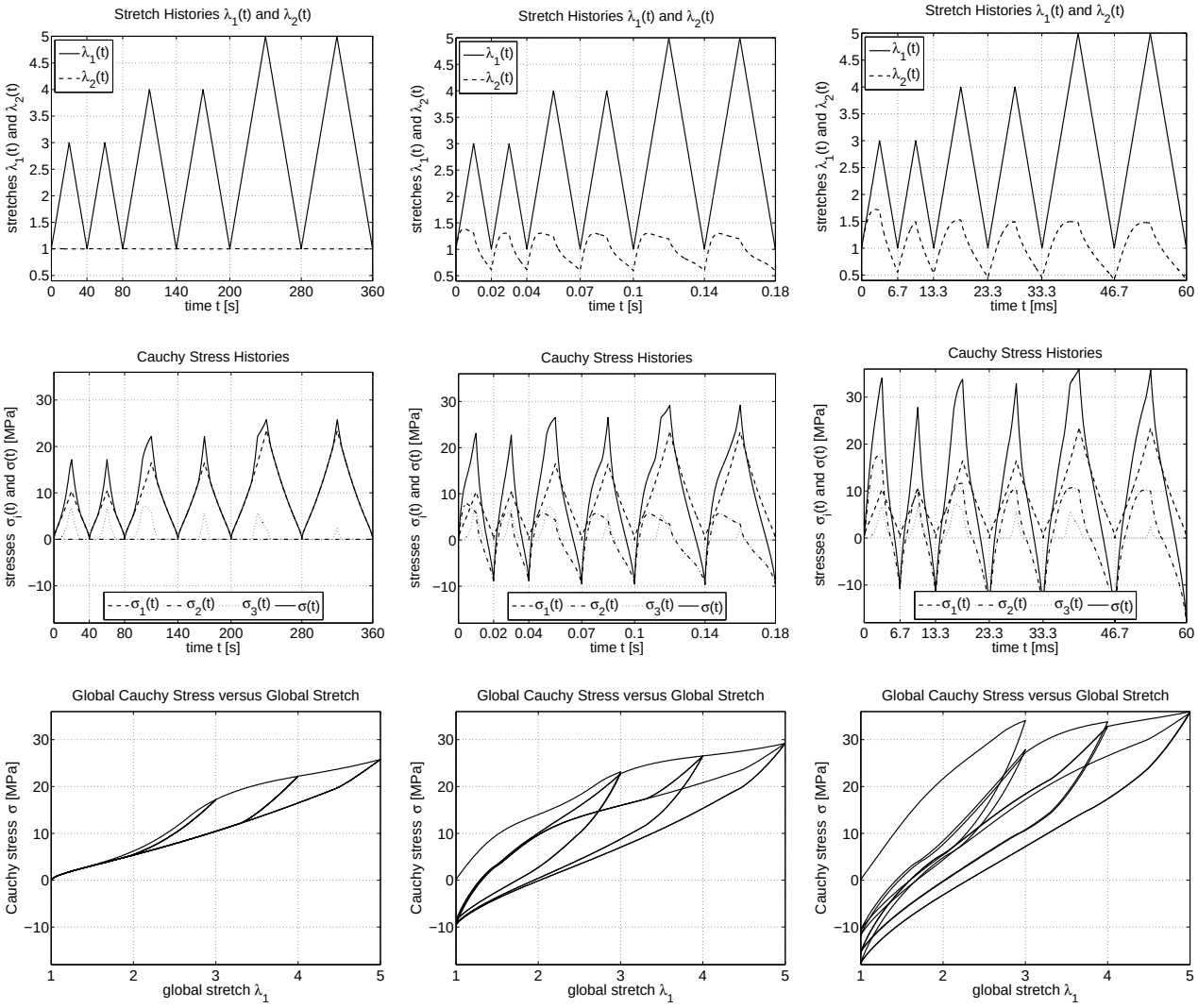

(a) Stretch rate $\dot{\lambda}_1 = 0.1\ \mathrm{s}^{-1}$ (b) Stretch rate $\dot{\lambda}_1 = 200\ \mathrm{s}^{-1}$ (c) Stretch rate $\dot{\lambda}_1 = 600\ \mathrm{s}^{-1}$

Figure 14: Model's behavior under the normalized loading at different stretch rates

Appendix A

Intermediate steps between equations (6) and (7) are detailed hereafter: equation (6) is pushed forward to the current configuration, in the usual way, to yield

$$\boldsymbol{\sigma}_j = \mathbf{F}_j \frac{\partial U_j}{\partial \mathbf{E}_j} \mathbf{F}_j^T + p_j \mathbf{I}. \tag{66}$$

The chain rule is then applied to $\partial U_j / \partial \mathbf{E}_j$, for instance in terms of the first two invariants of $\mathbf{C}_j$, i.e. $I_{\mathbf{C}_j} = \text{trace}(\mathbf{C}_j)$ and $II_{\mathbf{C}_j} = \frac{1}{2}\left(I_{\mathbf{C}_j}^2 - \text{trace}(\mathbf{C}_j^2)\right)$, as follows

$$\begin{aligned}
\frac{\partial U_j}{\partial \mathbf{E}_j} = 2\frac{\partial U_j}{\partial \mathbf{C}_j} &= 2\frac{\partial U_j}{\partial I_{\mathbf{C}_j}} \frac{\partial I_{\mathbf{C}_j}}{\partial \mathbf{C}_j} + 2\frac{\partial U_j}{\partial II_{\mathbf{C}_j}} \frac{\partial II_{\mathbf{C}_j}}{\partial \mathbf{C}_j} \\
&= 2\frac{\partial U_j}{\partial I_{\mathbf{C}_j}} \mathbf{I} + 2\frac{\partial U_j}{\partial II_{\mathbf{C}_j}} \left(I_{\mathbf{C}_j} \mathbf{I} - \mathbf{C}_j\right) \\
&= 2\left(\frac{\partial U_j}{\partial I_{\mathbf{C}_j}} + I_{\mathbf{C}_j} \frac{\partial U_j}{\partial II_{\mathbf{C}_j}}\right) \mathbf{I} - 2\frac{\partial U_j}{\partial II_{\mathbf{C}_j}} \mathbf{C}_j.
\end{aligned} \tag{67}$$

Recalling that tensors $\mathbf{b}_j$ and $\mathbf{C}_j$ have the same invariants, equation (7) is readily obtained by substituting expression (67) into (66) and rearranging terms.

Acknowledgments

This material is based upon work supported by the National Science Foundation under Grant No. NSF-CMMI-0900324. Any opinions, findings, and conclusions or recommendations expressed in this material are those of the authors and do not necessarily reflect the views of the National Science Foundation.

References

Ang, A., Tang, W., 2007. Probability concepts in engineering: emphasis on applications in civil & environmental engineering. Wiley.

Arruda, E. M., Boyce, M. C., 1993. A three-dimensional constitutive model for the large stretch behavior of rubber elastic materials. Journal of the Mechanics and Physics of Solids 41 (2), 389 – 412.

Bažant, P., Oh, B. H., 1986. Efficient numerical integration on the surface of a sphere. ZAMM - Journal of Applied Mathematics and Mechanics / Zeitschrift fr Angewandte Mathematik und Mechanik 66 (1), 37 – 49.

Bonet, J., Wood, R., 2008. Nonlinear Continuum Mechanics for Finite Element Analysis, 6th Edition. Cambridge University Press.

Boyce, M. C., Arruda, E. M., 2000. Constitutive models of rubber elasticity: a review. Rubber Chemistry and Technology 73 (3), 504 – 523.

Brown, J. D., 1997. Nonlinear dynamic behavior of filled elastomers at small strain amplitudes. Graduate Faculty of Rensselaer Polytechnic Institute, Ph.D. dissertation.

Chagnon, G., Verron, E., Gornet, L., Marckmann, G., Charrier, P., 2004. On the relevance of continuum damage mechanics as applied to the mullins effect in elastomers. Journal of the Mechanics and Physics of Solids 52 (7), 1627 – 1650.

Chagnon, G., Verron, E., Marckmann, G., Gornet, L., 2006. Development of new constitutive equations for the mullins effect in rubber using the network alteration theory. International Journal of Solids and Structures 43 (2223), 6817 – 6831.

Coleman, B. D., Gurtin, M. E., 1967. Thermodynamics with internal state variables. The Journal of Chemical Physics 47 (2), 597 – 613.

Coleman, B. D., Noll, W., 1963. The thermodynamics of elastic materials with heat conduction and viscosity. Archive for Rational Mechanics and Analysis 13, 167 – 178.

D'Ambrosio, P., De Tommasi, D., Ferri, D., Puglisi, G., Apr. 2008. A phenomenological model for healing and hysteresis in rubber-like materials. International Journal of Engineering Science 46 (4), 293 – 305.

Dargazany, R., Itskov, M., 2009. A network evolution model for the anisotropic mullins effect in carbon black filled rubbers. International Journal of Solids and Structures 46 (16), 2967 – 2977.

De Tommasi, D., Puglisi, G., Saccomandi, G., 2006. A micromechanics-based model for the mullins effect. Journal of Rheology 50 (4), 495 – 512.

Diani, J., Brieu, M., Vacherand, J., 2006. A damage directional constitutive model for mullins effect with permanent set and induced anisotropy. European Journal of Mechanics - A/Solids 25 (3), 483 – 496.

Diani, J., Fayolle, B., Gilormini, P., Mar. 2009. A review on the mullins effect. European Polymer Journal 45 (3), 601 – 612.

Dorfmann, A., Ogden, R., 2004. A constitutive model for the mullins effect with permanent set in particle-reinforced rubber. International Journal of Solids and Structures 41 (7), 1855 – 1878.

Dorfmann, A., Pancheri, F., 2012. A constitutive model for the mullins effect with changes in material symmetry. International Journal of Non-Linear Mechanics 47 (8), 874 – 887.

Drapaca, C. S., Sivaloganathan, S., Tenti, G., Oct. 2007. Nonlinear constitutive laws in viscoelasticity. Mathematics and Mechanics of Solids 12 (5), 475 – 501.
Drozdov, A. D., Dorfmann, A., 2004. A constitutive model in finite viscoelasticity of particle-reinforced rubbers. Meccanica 39 (3), 245 – 270.
Gent, A. N., 1996. A new constitutive relation for rubber. Rubber Chemistry and Technology 69 (1), 59 – 61.
Gillibert, J., Brieu, M., Diani, J., 2010. Anisotropy of direction-based constitutive models for rubber-like materials. International Journal of Solids and Structures 47 (5), 640 – 646.
Holzapfel, G., 2000. Nonlinear solid mechanics: a continuum approach for engineering. Wiley.
Hoo Fatt, M. S., Ouyang, X., 2007. Integral-based constitutive equation for rubber at high strain rates. International Journal of Solids and Structures 44 (20), 6491 – 6506.
Hoo Fatt, M. S., Ouyang, X., 2008. Three-dimensional constitutive equations for styrene butadiene rubber at high strain rates. Mechanics of Materials 40 (12), 1 – 16.
Horgan, C. O., Ogden, R. W., Saccomandi, G., 2004. A theory of stress softening of elastomers based on finite chain extensibility. Proceedings of the Royal Society of London. Series A: Mathematical, Physical and Engineering Sciences 460 (2046), 1737 – 1754.
Huber, N., Tsakmakis, C., 2000. Finite deformation viscoelasticity laws. Mechanics of Materials 32 (1), 1 – 18.
Itskov, M., Haberstroh, E., Ehret, A., Vhringer, M., 2006. Experimental observation of the deformation induced anisotropy of the mullins effect in rubber. Kautschuk Gummi Kunststoffe 3, 93 – 96.
Kachanov, L., 1986. Introduction to Continuum Damage Mechanics. Vol. 10 of Mechanics of Elastic Stability. Dordrecht, Boston: M. Nijhoff.
Lemaître, J., 1996. A course on damage mechanics. Springer.
Lin, R., Schomburg, U., 2003. A finite elastic-viscoelastic-elastoplastic material law with damage: theoretical and numerical aspects. Computer Methods in Applied Mechanics and Engineering 192 (1314), 1591 – 1627.
Lion, A., 1996. A constitutive model for carbon black filled rubber: Experimental investigations and mathematical representation. Continuum Mechanics and Thermodynamics 8, 153 – 169.
Liu, M., 2010. Constitutive equations for the dynamic response of rubber. The Graduate Faculty of The University of Akron, Ph.D. dissertation.
Liu, M., Hoo Fatt, M. S., 2011. A constitutive equation for filled rubber under cyclic loading. International Journal of Non-Linear Mechanics 46 (2), 446 – 456.
Machado, G., Chagnon, G., Favier, D., 2010. Analysis of the isotropic models of the mullins effect based on filled silicone rubber experimental results. Mechanics of Materials 42 (9), 841 – 851.
Machado, G., Chagnon, G., Favier, D., 2012. Induced anisotropy by the mullins effect in filled silicone rubber. Mechanics of Materials 50 (0), 70 – 80.
Marckmann, G., Verron, E., 2006. Comparison of hyperelastic models for rubberlike materials. Rubber Chemistry and Technology 79 (5), 835 – 858.
Marckmann, G., Verron, E., Gornet, L., Chagnon, G., Charrier, P., Fort, P., 2002. A theory of network alteration for the mullins effect. Journal of the Mechanics and Physics of Solids 50 (9), 2011 – 2028.
Miehe, C., Keck, J., 2000. Superimposed finite elasticviscoelasticplastoelastic stress response with damage in filled rubbery polymers. experiments, modelling and algorithmic implementation. Journal of the Mechanics and Physics of Solids 48 (2), 323 – 365.
Mullins, L., 1969. Softening of Rubber by Deformation. Rubber chemistry and technology. Rubber Division, American Chemical Society.
Ogden, R. W., Roxburgh, D. G., 1999. A pseudoelastic model for the mullins effect in filled rubber. Proceedings of the Royal Society of London. Series A: Mathematical, Physical and Engineering Sciences 455 (1988), 2861 – 2877.
Pioletti, D. P., Rakotomanana, L. R., Benvenuti, J. F., Leyvraz, P. F., 1998. Viscoelastic constitutive law in large deformations: application to human knee ligaments and tendons. Journal of Biomechanics 31 (8), 753 – 757.
Roland, C. M., 2006. Mechanical behavior of rubber at high strain rates. Rubber Chemistry and Technology 79 (3), 429 – 459.
Yeoh, O. H., 1990. Characterization of elastic properties of carbon-black-filled rubber vulcanizates. Rubber Chemistry and Technology 63 (5), 792 – 805.